ChemPubSoc Europe

DOI: 10.1002/chem.201601187

CHEMISTRY A European Journal Full Paper

Molecular Electronics

Multiscale Approach to the Study of the Electronic Properties of Two Thiophene Curcuminoid Molecules

Alvaro Etcheverry-Berríos,[a] Ignacio Olavarría,[b] Mickael L. Perrin,[b] Raúl Díaz-Torres,[c] Domingo Jullian,[a] Ingrid Ponce,[d] José H. Zagal,[d] Jorge Pavez,[d] Sergio O. Vásquez,[a] Herre S. J. van der Zant,[b] Diana Dulić,*[e] Núria Aliaga-Alcalde,*[f] and Monica Soler*[a]

Abstract: We studied the electronic and conductance properties of two thiophene–curcuminoid molecules, 2-thphCCM (**1**) and 3-thphCCM (**2**), in which the only structural difference is the position of the sulfur atoms in the thiophene terminal groups. We used electrochemical techniques as well as UV/Vis absorption studies to obtain the values of the HOMO–LUMO band gap energies, showing that molecule **1** has lower values than **2**. Theoretical calculations show the same trend. Self-assembled monolayers (SAMs) of these molecules were studied by using electrochemistry, showing that the interaction with gold reduces drastically the HOMO–LUMO gap in both molecules to almost the same value. Single-molecule conductance measurements show that molecule **2** has two different conductance values, whereas molecule **1** exhibits only one. Based on theoretical calculations, we conclude that the lowest conductance value, similar in both molecules, corresponds to a van der Waals interaction between the thiophene ring and the electrodes. The one order of magnitude higher conductance value for molecule **2** corresponds to a coordinate (dative covalent) interaction between the sulfur atoms and the gold electrodes.

Introduction

Molecular electronics is a field of nanoscience and nanotechnology that consists of studying single molecules, or nanoscale collections of single molecules, as electronic components at the molecular level. It focuses on the ability to tune the intrinsic properties of molecules[1] for better device performance. During the last decade, a number of organic species and coordination compounds have been proposed and their electronic and charge transport properties have been studied in the context of single-molecule-based devices.[2] Factors such as the length,[3] conjugation,[4] conformation,[5a] or even changes in the planarity of the molecule,[5] and anchoring groups[6] of the molecule under study, are crucial for achieving reliable electronic devices with desirable performance.[7] In particular, several studies have been centered on understanding the effect that different anchoring groups can have on the conductance in a single-molecule device, anchoring groups such as HS,[3b,8a–d] COOH,[8a,e] NH_2,[3b,c,8] MeS,[8f,g] Me_2P,[3c,8f] MeSe,[8i] thiophene,[8h,9a] selenophene,[8i] tripodal anchors with pyridine rings,[9b] pyridine,[3b,8d,e] CN,[3b,8d,e] benzo-hydrothiophene,[3b,8d,i] SO_3^-,[8e] OH,[8e] alkyne,[8c,d] NO_2,[8d,i] and benzothiophene.[8d,j] Thus, establishing a relationship between the intrinsic molecular properties and device performance is a central task for developing reliable molecular electronic devices.

In this work, we investigate the electrochemical and single-molecule charge-transport properties of two thiophene-terminated curcuminoid (CCMoid) molecules, 2-thphCCM (**1**) and 3-thphCCM (**2**) (Figure 1). In particular, we have investigated the influence of the sulfur atom positions on the electronic and charge-transport properties of molecules **1** and **2**. These two molecules have the same atomic composition, the same anchoring groups with sulfur atoms (S) as linkers, but differ in the position of the terminal anchoring groups, providing molecule **2** with the S atoms more available (outer posi-

[a] *A. Etcheverry-Berríos, D. Jullian, Dr. S. O. Vásquez, Dr. M. Soler*
Departamento de Ciencia de los Materiales
Facultad de Ciencias Físicas y Matemáticas
Universidad de Chile, Beaucheff 851, Santiago (Chile)
E-mail: msoler@ing.uchie.cl

[b] *I. Olavarría, Dr. M. L. Perrin, Dr. H. S. J. van der Zant*
Kavli Institute of Nanoscience, Delft University of Technology
Lorentzweg 1, 2628 CJ Delft (The Netherlands)

[c] *R. Díaz-Torres*
Departament de Química Inorgànica
Universitat de Barcelona-ICMAB
(Institute of MaterialsScience of Barcelona)-CSIC
Diagonal 645, 08028 Barcelona (Spain)

[d] *Dr. I. Ponce, Dr. J. H. Zagal, Dr. J. Pavez*
Facultad de Química y Biología, Universidad de Santiago de Chile
Av. Libertador Bernardo Ohiggins 3363, Estación Central, Santiago (Chile)

[e] *Dr. D. Dulić*
Departamento de Física, Facultad de Ciencias Físicas y Matemáticas
Universidad de Chile, Av. Blanco 2008, Santiago (Chile)
E-mail: ddulic@ing.uchile.cl

[f] *Dr. N. Aliaga-Alcalde*
ICREA Researcher (Institució Catalana de Recerca i Estudis Avançats)
at the ICMAB-CSIC
Campus de la Universitat Autònoma de Barcelona
08193, Bellaterra (Spain)
E-mail: nuria.aliaga@icrea.cat

Supporting information and ORCID number from the author for this article is available on the WWW under http://dx.doi.org/10.1002/chem.201601187.

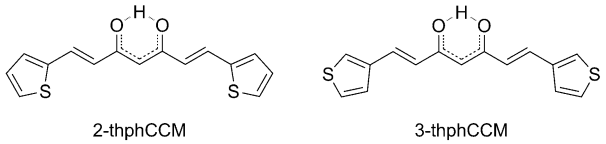

Figure 1. Thiophene-curcuminoid molecules, 2-thphCCM (**1**) and 3-thphCCM (**2**).

tion) for anchoring to gold electrodes than molecule **1** (Figure 1).

To design ligands that are suitable for molecular electronics, we consider three principal aspects. First, our ligands must have proper anchoring groups to enable attachment to the electrodes; secondly, to achieve good molecular conductance, a short but highly conjugated skeleton is needed. Finally, our group is interested in study of the interplay between molecular conductance and magnetic properties, the latter achieved by metal complexation. In this sense, CCMoids were chosen because they possess a highly conjugated skeleton, have a β-diketone group that enables coordination, and their synthetic versatility allows the facile replacement of the aromatic groups with a wide library of commercial aldehydes with anchoring groups. These molecules represent promising building blocks for the construction of functional molecular nanocircuits as they possess structural flexibility and a well-developed synthetic chemistry methodology allowing their physical and chemical properties to be tailored. Both molecules share a β-diketone group placed in the center of a seven carbon conjugated chain, which allows coordination to metal ions,[10,11] such as Cu^{II}, Zn^{II}, Mn^{II}, V^{IV}, and Ru^{II},[10] as well as lanthanides Dy^{III}, Tb^{III}, Eu^{III}, Gd^{III}, and Lu^{III}.[11] This β-diketone moiety shows a tautomeric equilibrium between a diketo and a keto-enol form, and several studies have focused their attention to elucidate which of these forms is more stable. Spectroscopic studies[12] have shown that the *cis* keto-enol tautomer (Figure 1) is the more stable structure in solution and X-ray diffraction shows the same result in the solid state.[13] Specifically, the *cis* keto-enol tautomer has an intramolecular hydrogen-bond (KEIHB, keto-enol intramolecular hydrogen-bond), which could affect the molecular conductance by means of an intramolecular proton transfer. On the other hand, the two terminal carbon atoms of the conjugated carbon are bound to two terminal rings, which can be chosen from a wide library of terminal substituents. The side groups can also be easily modified to improve the electrical contact with the electrodes. In this respect, the anchoring groups chosen for our molecules are thiophene units, which have affinity to gold. When a thiophene groups binds a metal surface, the sulfur anchoring atom, which is in an aromatic ring, have two possible type of bonding interactions as it has two unpaired electrons. One of the unpaired electrons is delocalized on the aromatic ring, able to bind the gold surface though a π-interaction. On the other hand, the other unpaired electron can bind through a coordinate bond (dative covalent bond), in which the two electrons of the bond are donated from the sulfur atom to the surface.[14] Several examples of molecules with thiophene anchoring groups deposited between electrodes have been reported.[8h,9a] Recently, an anthracene-based CCMoid, called 9Accm, and a Cu^{II}-9Accm compound have been studied in molecular break junction devices made of a few layers of graphene (FLG).[15] To the best of our knowledge, charge-transport studies of CCMoids using gold electrodes have not been reported yet.

First, we study, in the bulk, different ways to obtain experimentally and theoretically the frontier orbitals and HOMO–LUMO band gap[16] energies of these two curcuminoid molecules in the gas phase, in solution, and in the solid state. Generally speaking, the difference in conductance between two molecules can be predicted based on the difference in the band gap energy, although this band being near the Fermi level (5.1 eV) is also important.[17] As a first approximation, a small HOMO–LUMO gap energy is beneficial for the molecular conductance properties. However, it is known that the frontier orbital energies will change based on the hybridization of these orbital wave functions with those of the metallic leads in the electronic device.[8c–e] We have performed electrochemical studies on self-assembled monolayers of these molecules to understand how the frontier orbitals and HOMO–LUMO band gap energies can change as a result of the molecule–surface interaction. Finally, we have performed conductance studies by using a mechanically controlled break junction (MCBJ) device in the electrode–molecule–electrode configuration. We support our findings by DFT calculations.

Results and Discussion

Compounds **1** and **2**, shown in Figure 1, were synthesized by a modified version of the Pabon method.[18] A precise description of this methodology is given in the experimental section; the characterization by FTIR, ^{1}H and ^{13}C NMR spectroscopies of both systems is depicted in the Supporting Information. The structural difference between both molecules regarding the position of the S atoms is mentioned above. Such difference may influence not only their electronic and charge-transport properties but also their binding abilities toward the surface of the electrode. To determine the difference in energy of these frontier orbitals, we have performed measurements on the macroscopic scale, including electrochemical studies in solution (differential pulse voltammetry) and UV/Vis spectra in solution and in the solid state.

Electrochemical studies in solution

Cyclic voltammetry (CV) and differential pulse voltammetry (DPV) were used to investigate the redox properties of **1** and **2** and to estimate values of the HOMO and LUMO energy levels of both systems. Figure 2 shows the CV and DPV experiments and the electrochemical data are summarized in Table S1 (in the Supporting Information). Overall, the two compounds display a similar electrochemical behavior, exhibiting a number of irreversible reductions in the −2.5 to −1.5 V region and three close irreversible oxidations in the +0.5 to +2.0 V range (Figures S8–S10 in the Supporting Information), with features that

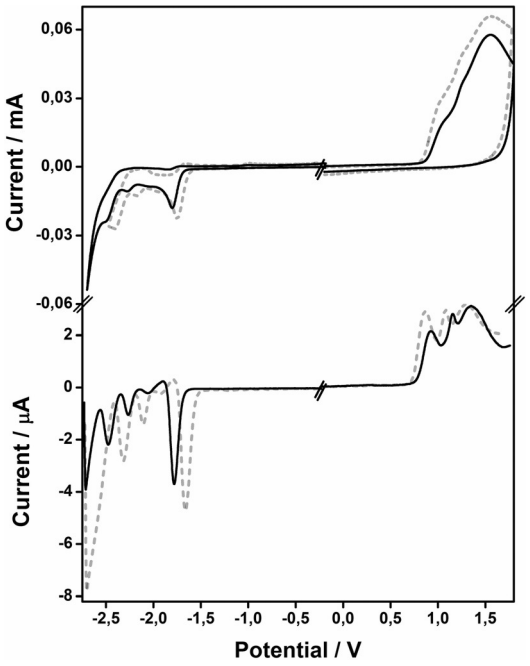

Figure 2. Cyclic voltammograms (CV) (top) and differential pulse voltammograms (DPV) (bottom) of **1** (dashed line) and **2** (solid black line). Measurements were conducted under N_2, in dry CH_2Cl_2 containing 0.1 M tetrabutylammonium hexafluorophosphate [TBA(PF_6)] as supporting electrolyte. Potentials vs. Fc/Fc^+.

are similar to other thiophene species reported in the literature.[19] However, a closer look at the DPV data shows that the potentials for the first oxidation and reduction processes are shifted between **1** and **2** (Table S1). Compound **1** presents the first oxidation and reduction processes at +0.87 and −1.66 V, respectively, whereas **2** displays these processes at +0.95 and −1.80 V (both referenced vs. Fc/Fc^+).

The HOMO is estimated[20a,b] from the first oxidation potential, corresponding to the ionization potential (IP; removal of one electron from the highest occupied molecular orbital) and the LUMO is deduced from the first reduction potential, correlated with the electron affinity (EA; addition of one electron to the lowest unoccupied orbital). To proceed with the calculations and to compare the experimental values with previous published data, one has to consider that the Fc/Fc^+ couple has a potential of 4.80 eV below the vacuum level.[20b,c] Therefore, the HOMO and LUMO energy levels (E_{HOMO} and E_{LUMO}) of both molecules can be calculated according to the following equations:

$$E_{HOMO} = -(E_{onset(ox)} + 4.8)\ \text{eV} \quad (1)$$

and

$$E_{LUMO} = -(E_{onset(red)} + 4.8)\ \text{eV} \quad (2)$$

so that

$$E_g = E_{onset(ox)} - E_{onset(red)}\ \text{(eV)} \quad (3)$$

in which $E_{onset(ox)}$ and $E_{onset(red)}$ are the onset[20d] potentials for the oxidation and reduction of **1** and **2** determined from the DPV experiments (vs. Fc/Fc^+).

As a result, the corresponding HOMO and LUMO energy levels are −5.53 and −3.26 eV for **1**, and −5.58 and −3.11 eV for **2** (Table S2 in the Supporting Information). Hence, the electrochemical band gaps, E_g^{ec}, are 2.27 and 2.47 eV, respectively. Additional calculations relate the electrochemical data to the saturated calomel electrode (SCE)[20e] and use the appropriated formulae[20b] to provide similar values (see Table S2). These energies as well as the gap values are comparable to other conjugated systems, which are of the order of donor polymers and small molecules.[19,20a–c] For both molecules, the metal Fermi level is found to lie closer to the HOMO than to the LUMO energy level.

Optical studies

The electronic absorption spectra of both molecules in the solid state (Figure S11 in the Supporting Information) were used to obtain the HOMO–LUMO gap of the molecules, which are summarized in Table 1. The UV/Vis and emission spectra of both compounds are consistent with the properties expected for this class of compounds. In both compounds, the *cis* keto-enol configuration has an intramolecular hydrogen-bond (KEIHB), which increases the delocalization of the π-system.[12e] The strength of the hydrogen-bond is highly correlated with the degree of delocalization of the π-system; in a more delocalized system, the strength of the hydrogen-bond decreases. Even though **1** and **2** show a similar shape when comparing their absorbance spectra, there is a reduction in the absorption area and a clear blueshift of the maxima band of approximately 20 nm going from system **1** to **2** (Figure S11). Such a shift is associated with the aromatic nature of the 2-thiophene and 3-thiophene groups, in which the conjugation is less extended over the thiophene rings in molecule **2**. The assignment of the band in the 400 nm region is attributed to π→π* transitions, which also account for the high-energy bands in the 200–270 nm range.[12d,21] Based on the absorption spectra obtained for **1** and **2**, the optical band gap of the frontier orbitals (E_g^{op}) were estimated by using the cutoff (onset) of the lowest absorbed energy in their respective UV/Vis spectra. The E_g^{op} for

Table 1. Comparison of band gap energies [eV] of molecule **1** and **2** in the gas, solution, and solid phases.

	1	**2**
E_g^{theor} gas phase[a]	5.72	5.96
E_g^{theor} solution phase[a]	3.08	3.26
E_g^{op} [eV] solid[b]	2.20	2.45
E_g^{ec} [eV] solution[c]	2.27	2.47

[a] Obtained from theoretical calculations. [b] Calculated from UV/Vis measurements. [c] Calculated from electrochemical data.

the solid provided values of 2.20 eV for 2-thphCCM (**1**) and 2.45 eV for 3-thphCCM (**2**).

As for the fluorescence emission (Figure S13 in the Supporting Information), compound **2** shows lower intensity when measured at the same conditions as **1**. This difference can be related to the fact that, as previously reported,[12e,22] curcuminoids have a radiationless decay mechanism through direct excited-state intramolecular proton transfer (ESIPT) from the enol to the keto group in the *cis* keto-enol tautomer. The rate of the ESIPT process is faster if the intramolecular hydrogen-bond is stronger, which correlates with our systems. Molecule **2** shows an increase in the strength of KEIHB, because it is less delocalized, with a stronger hydrogen-bond, thus it shows a decrease in the fluorescence intensity.

DFT calculations in the gas phase and solution

To calculate the HOMO–LUMO gap, we have run two sets of calculations: the first one is a set of density functional theory calculations (DFT) in the gas phase based on the Kohn–Sham analog of the Koopmans' theorem (KT, valid within the Hartree–Fock framework),[23a] which were demonstrated by Gritsenko and Baerends[23b–c] and expanded to other problems.[23d] The second group of DFT calculations include the effect of solvent (CH_2Cl_2) and Tomasi's continuum polarizable method in order to compare the results with experimental measurements from the UV/Vis spectra.

In both cases, the calculations are a reasonably good estimation of the HOMO–LUMO gap and the absorption spectral characteristics, but we cannot expect a perfect agreement with the experimental data, as the calculations are affected by the limits of the theoretical approach,[23b] the choice of the exchange-correlation functional, and the basis set.

In this work, we consider the B3LYP hybrid functional, consistent with B3 Becke's three-parameter exchange correlation functional, and the Lee, Yang, and Parr LYP correlation functional that recovers the dynamic electron correlation.[24] This choice was made by consideration of our previous work[25,26] with conjugated molecules. The well-known popularity of the B3LYP functional within the theoretical community is due to calculations with results that are comparable to most post-Hartree–Fock methods but obtained in a faster way. On the other hand, the 6-311G+(d,p) basis set is the rather complete set of 6-311G functions[27] supplemented with diffuse functions[28] as well as polarization[29] and is used to have a better representation of the wave functions of the molecular systems. In summary, the DFT/B3LYP/6-311G+(d,p) methodology chosen for this part of the study could be useful to compare results and predictions from and for other authors as well as our own previous results and, as mentioned in the following paragraphs, give good results on a quantitative basis. Strictly speaking, the choice of the best exchange-correlation functional, and the basis set for a given problem is by itself a complete and separate study that exceeds the scope of this work.

Table 1 shows the calculated band gap energies for the molecules in the gas phase and in solution (Table S3 in the Supporting Information). The HOMO and LUMO data calculated, including the solvent effect, show quite good agreement with the experimental data from the UV/Vis experiments in solution (Figure S11). Based on the comparison of the calculated band gap energies of both molecules, molecule **1** has smaller energies than **2**. The band gap energies for both molecules obtained from solid-state optical absorption or solution electrochemistry are in agreement. All the energies obtained for **1** and **2** show the same trend, suggesting to a first approximation that molecule **1** could conduct better.

Representations of the molecular orbitals for the HOMO and LUMO electronic states for compound **1** and **2** are presented in Figure 3, which show the typical delocalization of the

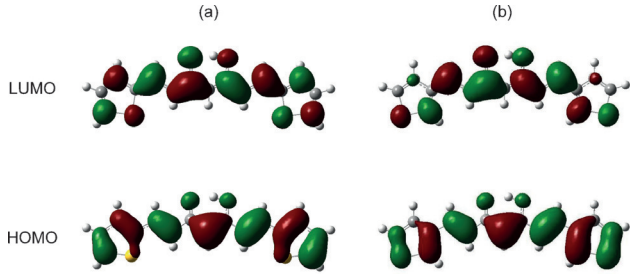

Figure 3. Molecular orbitals of a) 2-thphCCM (**1**) and b) 3-thphCCM (**2**).

charge of a conjugated molecule, using π-type orbitals along the complete structure. Two observations can be made when comparing the molecular orbitals of **1** and **2**: (i) molecule **1** has a reduced capacity for eventual charge transfer as the S atoms are less involved in the HOMO orbital, (ii) looking at the LUMO orbital, molecule **2** is less conjugated, as two carbon atoms of each thiophene ring are not participating in the conjugation of the complete structure, which gives a more direct path for eventual charge transport from one sulfur atom to the other in the molecule, favoring better conductance. Therefore, depending on if the charge transport is through the HOMO or the LUMO orbital, the conductance of both molecules could be different. Based on the proximity of the HOMO energies of both molecules, as obtained from electrochemistry, with the Fermi level of gold, as a first approximation, the injection could be through the HOMO.

To study how these molecular frontier orbital energies change with the orbitals mixing in two dimensions in a molecule–gold electrode interaction, we performed electrochemical studies on self-assembled monolayers (SAMs).

Electrochemical studies on SAMs

Electrochemical studies of self-assembled monolayers (SAMs) of **1** and **2** on Au(111) were also carried out to evaluate the changes in the HOMO and LUMO energy levels. The results are summarized in Table 2. The experimental conditions used were the same as for the bulk electrochemical measurements discussed above. The formation of SAMs was confirmed through the observation of reductive desorption processes of the SAMs from the Au(111) surfaces, corroborating the chemisorption be-

Table 2. Electrochemical data in CH_2Cl_2 for molecules **1** and **2** in solution and in SAMs. Potentials [V] (DPV data) are referenced to Fc/Fc^+. E_{HOMO} and E_{LUMO} [eV] refer to the HOMO and LUMO energy levels, E_g^{elec} [eV] stands for the electrochemical energy gap.

	1 st Oxid.	1 st Red.	E_{HOMO}	E_{LUMO}	E_g^{elec}
1 Sol.	+0.87	−1.66	−5.53	−3.26	2.27
2 Sol.	+0.95	−1.80	−5.58	−3.11	2.47
1 SAM	+0.78	−0.33	−5.40	−4.65	0.75
2 SAM	+0.93	−0.30	−5.42	−4.68	0.74

tween the thiophene sulfur atoms and the gold surface.[30] Cyclic voltammetry measurements were conducted for both self-assembled systems, SAM(2-thphCCM-Au(111)) for **1** and SAM(3-thphCCM-Au(111)) for **2**. Two oxidation and four reduction processes are present in both SAMs, as shown in Figure 4.

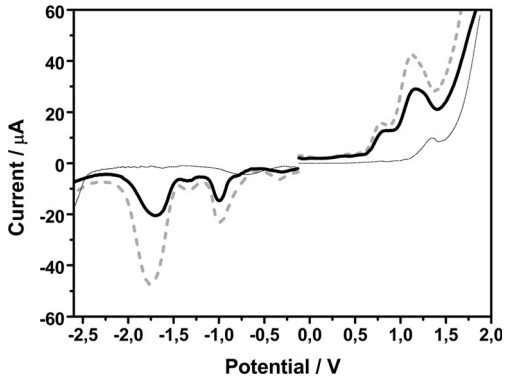

Figure 4. Differential pulse voltammograms (DPV) for Au(111) modified with SAMs of **1** (dashed line) and **2** (solid black line). The black dotted line represents Au(111) without either of the molecules. Measurements were conducted under N_2, in dry CH_2Cl_2 containing 0.1 M $TBA(PF_6)$ as supporting electrolyte. Potentials were reference to Fc/Fc^+.

The redox behavior of SAM(2-thphCCM-Au(111)) was similar to SAM(3-thphCCM-Au(111)), and the redox processes for the oxidation and reduction in both systems are much closer than those found in solution (Figure 2). As before, differential pulse voltammetry (DPV) provided a better resolution of the redox processes.

SAM(2-thphCCM-Au(111)) for **1** presents the first oxidation and reduction processes at +0.78 and −0.33 V, respectively, and SAM(3-thphCCM-Au(111)) for **2** displays parallel redox processes at +0.93 and −0.30 V. The comparison of these potentials with the ones obtained for the molecules in solution suggests that the oxidation potentials for the SAM configurations have experienced small shifts toward positive values, whereas the reduction potentials show pronounced shifts to less negative values.

Shifts of the redox processes for compounds anchored to the Au surface, compared with their electrochemical processes in solution, have been previously observed for thiophene alkane thiol and terthiophene-derived SAMs on gold surfaces.[31] Overall, the oxidation potential processes are similar in both experiments, that is, in solution and as SAMs attached to Au. In contrast, there is a big difference between the reduction potentials of both molecular SAMs and their corresponding molecular potentials in solution, with molecular SAMs reduction values very close to each other (−0.3 V (**1**) and −0.33 V (**2**)).

The energy gap between the HOMO and LUMO energy levels was calculated by using the same methodology as introduced for the electrochemical experiments in solution (see the Supporting Information). We found that the electrochemical band gaps, for example, for **1** and **2** when in contact with the gold electrode, are 0.75 and 0.74 eV, respectively. This change in the band gap energies upon binding is mainly a result of the mixing of the LUMO orbitals with the orbitals of the gold electrode, as the HOMO orbitals are almost the same for both molecules. When compounds **1** and **2** are anchored to the gold surface, the reduction potentials (or the LUMO energies) cause the reduction of the band gap energy, resulting in smaller values than the ones obtained for the molecules in solution. Comparing the frontier orbital energies with the reported Fermi energy of gold electrodes (5.1 eV),[17] we see that the later falls in between the HOMO and LUMO energy levels of both molecules (Table 2), suggesting that these molecules may show conductance if a single-molecule device is constructed. Based on the electrochemical measurements of SAMs, we can conclude that the interaction with the gold electrodes reduces the LUMO energies of both molecules, ending up with a smaller and more similar band gap for both molecules, therefore as a first approximation, if everything else is the same, both molecules will show similar conductance values in a single-molecule device with gold electrodes.

Single-molecule conductance measurements

Single-molecule conductance measurements were performed with the controllable mechanical break junction technique (MCBJ).[32] A drop of the molecular solution was deposited on the device before breaking the electrode and thousands of molecular conductance traces were collected while separating these electrodes, allowing a statistical investigation to be performed by building one-dimensional and two-dimensional conductance histograms. Figure 5 displays two-dimensional conductance versus electrode displacement histograms (G versus the electrode displacement d in logarithmic scale) of a MCBJ with compound **1** (Figure 5a) and **2** (Figure 5b). In these histograms, individual breaking traces have been shifted along the horizontal electrode displacement axis to fix the rupture of the one-atom gold contact at zero. Areas of high counts represent the most typical breaking behavior of the molecular junctions. The insets contain the histograms with all breaking traces; the main figures show the ones built up from selected traces. In the latter case, the shortest and steepest traces have been omitted so that most of the tunneling traces in which there are no molecular signatures are not taken into account.

The two-dimensional histograms (Figure 5) show that for compound **1**, there is a region of high counts between 10^{-4} and 10^{-5} G_0 and for compound **2**, there are two regions of high counts, one just above 10^{-4} G_0 and one just below

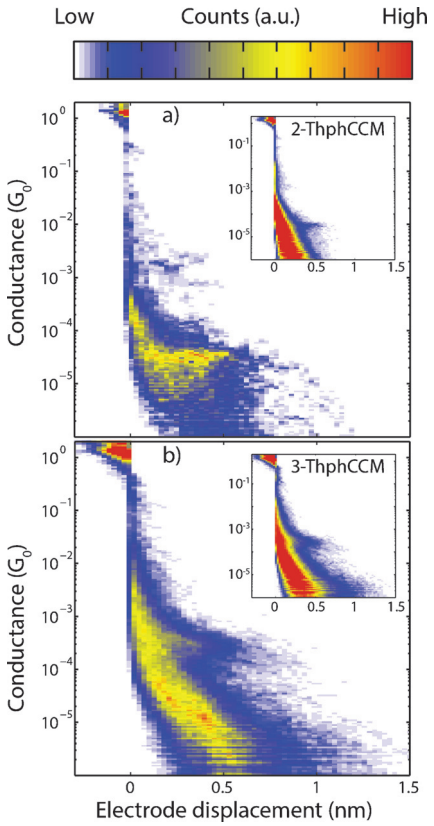

Figure 5. Conductance versus electrode displacement two-dimensional histogram constructed with a) 171 traces for molecule **1** and b) 1299 traces for molecule **2**. The selected traces are the ones, in which the distance between the point at which the trace drops below 1 G_0 and the last point, in which the conductance is larger than 1×10^{-5} G_0, which is longer than 0.4 nm. The insets display the histograms without data selection constructed by using 5000 traces.

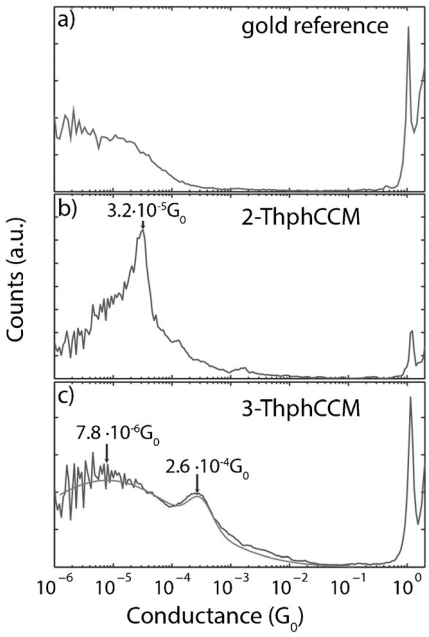

Figure 6. Logarithmically binning one-dimensional conductance histograms of a) the clean gold reference sample without data selection (same junction as that presented in Figure 5 b, same results) and b) selected traces from Figure 5 of 2-thphCCM (**1**) and c) 3-thphCCM (**2**). The light-gray line (lower panel) corresponds to a lognormal fitting of the two conductance peaks.

10^{-5} G_0. A 2D histogram of the junction used to acquire the data in Figure 5 b prior to molecule deposition is shown in Figure S14 (in the Supporting Information). Such reference measurements were performed on all junctions to check that the bare gold junction was clean as evident from the presence of tunneling curves in the absence of additional features.

To extract the conductance values of the most probable molecular configuration, one-dimensional conductance histograms have been constructed. These 1D histograms and that of the reference without molecules are presented Figure 6. All three panels in this figure show, just before the rupture of the gold wire, the presence of clear steps at integer values of 1 G_0 ($G_0 = 2e^2/h = 77$ μS), the quantum of conductance. The histograms for the two molecules yield a distribution of conductance values peaked around 3×10^{-5} G_0 for **1** (Figure 6 b) and two conductance peaks at 3×10^{-4} G_0 and 8×10^{-6} G_0 for **2** (Figure 6 c).

Comparison of both histograms yields a consistent picture in which molecule **1** exhibits one stable conformation with a conductance plateau around 3×10^{-5} G_0, with counts concentrated for electrode displacements between 0 and 0.7 nm, with almost no counts at larger displacements. For molecule **2**, the histograms reveal a maximum around 3×10^{-4} G_0 and a broad maximum around 8×10^{-6} G_0, with counts spread over larger displacements, and conductance counts up to 1.2 nm electrode displacement. Figure 1 shows that the observed differences have to be related to the different positions of the sulfur atoms in the terminal thiophene rings. If we compare the distance between the sulfur atoms in both molecules, molecule **1** has the shortest distance between them and the observed conductance counts for molecule **2** at higher electrode displacement is thus consistent with the molecular structure. Moreover, the lower conductance value (Figure 6), which corresponds to a more stretched conformation of the molecule between the electrodes, is of the same order in both molecules, suggesting that the change in the sulfur atom position for that conformation does not affect the conductance considerably. The high conductance value seen only for molecule **2**, may then be related to the fact that molecule **2** has the S atoms at a more favorable position for anchoring to the gold electrodes, which is better for charge injection. To provide more insight into these different conformations, theoretical calculations were performed on molecules **1** and **2** between gold electrodes.

DFT calculations for the electrode–molecule–electrode configuration

To compare the single-molecule conductance measurements with theoretical calculations, we have calculated the transmission through molecules **1** and **2** by using the non-equilibrium Green's function method with a density functional theory (DFT) calculation of the ground-state electron density for dif-

ferent electrode stretching distances. We found that the exact geometry of the molecule with respect to the electrodes plays an important role in the HOMO and LUMO energy values, as well as on the transmission through the molecular junction. To investigate the evolution of the molecular conformation while stretching the junction, we performed DFT calculations for various electrode separations. For more details, see the Experimental Section.

In Figure 7, we present the different molecular junction configurations for molecules **1** and **2** during stretching. These

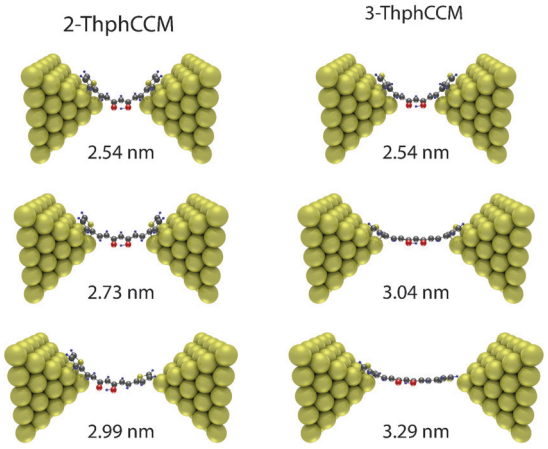

Figure 7. DFT calculations of the different molecular junction configurations. Top: initial molecular junction configuration; middle: the configuration at an intermediate stretch; bottom: the configuration at the point of maximum stretching for molecules **1** and **2**.

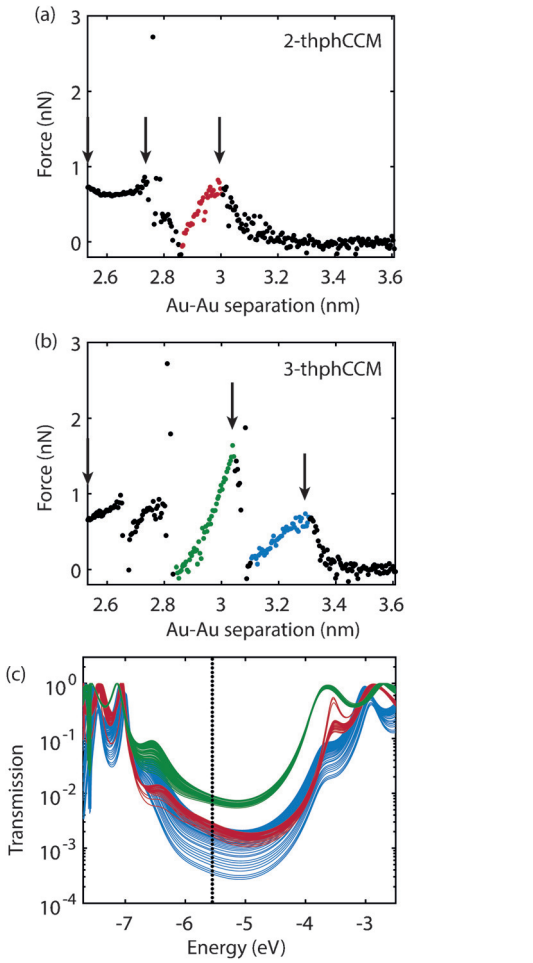

Figure 8. Force versus Au–Au distance curves as obtained from the DFT stretching calculations for molecule **1** (a) and molecule **2** (b). c) Transmission curves calculated by using DFT + NEGF for the molecules **1** and **2**. The colors of the curves are related to the junction geometry along the stretching curves shown in a) and b). The vertical dotted line indicates the estimated location of the Fermi energy.

three configurations are marked in Figure 8a and b with arrows in the force versus Au–Au distance plots. The initial molecular junction configuration is presented on top, whereas the middle and lower configurations correspond to maxima in the forces/displacement curves. The colors in Figure 8a,b are linked to the transmission curves shown in Figure 8c. These were calculated by using DFT + Σ in combination with the non-equilibrium Green's function (NEGF) formalism. Conductance values were then calculated by using the Landauer formula.[33]

Comparing the force–stretching curves for both molecules with the force maxima marked by the black arrows in Figure 8 and the representation of the calculated molecular junction configurations shown in Figure 7, the following observations can be made: first, the rupture of the molecular junction, that is, the last local maximum in the force, marked by the black arrows, occurs at 2.99 nm for molecule **1**, whereas molecule **2** can be stretched up to 3.29 nm, so essentially **2** can be stretched more than **1**. This may explain the shorter conductance plateaus for molecule **1** in the experimental conductance histograms. Second, the junction evolution for the two molecules is different. Molecule **1** shows a second peak at 2.74 nm, with an amplitude of 0.8 nN. Molecule **2**, on the other hand, shows multiple peaks, located at 2.62, 2.73, and 3.04 nm, with amplitudes of 0.9, 0.9, and 1.6 nN, respectively. The fact that the force is twice as high for the peak at 3.04 nm suggests a different nature for this bond compared with the others. Inspection of the different junction geometries in Figure 7 suggests the following scenarios: (i) at the point of rupture of molecule **1**, the interaction is a weak van der Waals interaction between a distant thiophene ring and the electrode, leaving only a H atom of the ring as the last contact with the gold electrode. No coordinate S–Au bond is formed, and the molecule/electrode interaction occurs through van der Waals forces. The peak at 2.73 nm is also caused by van der Waals forces, with the entire thiophene rings interacting with the electrodes. (ii) In the case of molecule **2**, the situation is different. At the point of rupture (3.29 nm), the hydrogen atom is the closest to the electrode suggesting a molecule/electrode interaction occurring through van der Waals forces. This is similar to molecule **1**. At positions 2.64 and 2.73 nm, the thiophene rings overlap with the gold electrodes and van der Waals forces predominate again. At a distance of 3.04 nm, however, the S atoms are located close to the gold, indicating the formation of coordinate bonds. This bond formation can be related to

the higher breaking force. Upon further stretching, as also seen in molecule **1**, the last molecule/electrode interaction is again through van der Waals forces.

This structural difference is also reflected in the transmission through the molecule while stretching, as shown in Figure 8c. For molecule **1**, when the molecular junction is formed through van der Waals interactions with the electrodes (red), the curves cluster around a conductance values of about 3×10^{-3} G_0. For molecule **2**, the conductance in the van der Waals regime (blue) is slightly lower than for molecule **1**, and with a larger spread. When molecule **2** is connected through the S atoms (green), on the other hand, the conductance is about an order of magnitude larger. The conductance values obtained from DFT are higher than the ones found in the MCBJ experiments, and can therefore only be compared qualitatively. Nevertheless, the two different binding geometries of molecule **2** yield different conductance values, with an order of magnitude difference between the two. In addition, the HOMO and LUMO energies of both molecules are similar to those obtained experimentally from the electrochemical measurements on SAMs.

Conclusion

The experimental data in solution and in the solid state show that the HOMO–LUMO band gap for molecule **1** has a lower energy value than for molecule **2**. Theoretical calculations show the same trend. Inspection of the HOMO and LUMO molecular orbitals show that both molecules have the typical delocalization of π-type orbitals along the complete structure of the molecule, but owing to the difference in the position of the sulfur atoms in the terminal thiophene rings, the electronic densities in the HOMO and LUMO orbitals are different. Analysis of the frontier molecular orbital electron densities suggest that if charge transport were to occur through the HOMO orbitals, molecule **1** could show a reduced capacity for eventual charge-transfer processes as the sulfur atom are less involved in the HOMO orbital. In the opposite case scenario, in which charge transport occurs through the LUMO energy levels of the molecules, molecule **2** shows a more direct path for eventual charge transport between both sulfur atoms, resulting in better conductance. Therefore, the energy band gap for molecule **1** is smaller than for **2**, but the electron energies of the HOMO and the LUMO orbitals may affect differently the injected process to or from the molecule. Once the molecules are anchored on the gold electrode surfaces, the band gap energies are significantly reduced, exhibiting a lowering of the LUMO orbital energies in both cases, and the band gap of both molecules end up almost the same. Single-molecule measurements show that the conductance of molecule **2** is an order of magnitude higher than the conductance of molecule **1**. Therefore, considering that the HOMO and LUMO energies are almost the same, we attribute this difference in conductance to the ability of molecule **2** to form coordinate interactions with the nanogold electrodes, owing to the more available position of the sulfur atoms. We supported our findings by DFT calculations.

Experimental Section

Chemical synthesis

The chemicals and solvents used were purchased from commercial sources and used without further purification, unless especially mentioned. All experiments were carried out under aerobic conditions by using commercial grade solvents.

Synthesis of ((1*E*,4*Z*,6*E*)-5-hydroxy-1,7-di(thiophen-2-yl)hepta-1,4,6-trien-3-one (2-thphCCM) (1): Acetylacetone (acac; 0.75 mL, 7 mmol) and B_2O_3 (0.35 g, 5 mmol) were dissolved in EtOAc. The reaction mixture was heated at 55 °C for 30 min until a white suspension was formed. Then, a solution containing 2-thiophenecarboxaldehyde (1.3 mL, 14 mmol) and tri-*tert*-butyl borate (8 mL, 28 mmol) in EtOAc was added to the reaction mixture and stirred for 3 h at 55 °C. After cooling down for 1 h, a solution of *n*-butylamine (0.4 mL, 4 mmol) in EtOAc was added dropwise, and the reaction mixture was stirred at room temperature for 2 d. At this point, a red precipitate was formed corresponding to the boron complex, which was filtered and suspended in water to break the complex. After a day, the pure ligand was filtered and dried under vacuum. Yield: 79%. ^{1}H NMR (400 MHz, $CDCl_3$): $\delta=15.87$ (s, 1H), 7.77 (d, $J=15.5$ Hz, 2H), 7.38 (d, $J=5.0$ Hz, 2H), 7.27 (d, $J=3.7$ Hz, 2H), 7.07 (dd, $J=5.0$, 3.7 Hz, 2H), 6.41 (d, $J=15.5$ Hz, 2H), 5.75 ppm (s, 1H); ^{13}C NMR (75 MHz, [D_6]DMSO): $\delta=182.59$, 139.91, 133.29, 132.13, 130.12, 128.84, 122.79, 101.62 ppm; IR (KBr): $\nu=3102$, 1619, 1508, 1419, 1162, 966, 856, 705 cm^{-1}; ESI-MS: $m/z=287$ $[M<\text{M->H}]^-$; elemental analysis calcd (%) for 2-thphCCM·0.5H_2O: C 60.8, H 4.01, S 21.6; found: C 60.8, H 4.18, S 21.6.

Synthesis of ((1*E*,4*Z*,6*E*)-5-hydroxy-1,7-di(thiophen-3-yl)hepta-1,4,6-trien-3-one) (3-thphCCM) (2): Acetylacetone (acac; 0.75 mL, 7 mmol) and B_2O_3 (0.35 g, 5 mmol) were dissolved in EtOAc. The reaction mixture was heated at 55 °C for 30 min until a white suspension was formed. Then, a solution containing 3-thiophenecarboxaldehyde (1.3 mL, 14 mmol) and tri-*tert*-butyl borate (8 mL, 28 mmol) in EtOAc was added to the reaction mixture, and stirred for 3 h at 55 °C. After cooling down for 1 h, a solution of *n*-butylamine (0.4 mL, 4 mmol) in EtOAc was added dropwise, and stirred at room temperature for 2 d. At this point, an orange precipitate was formed, which was filtered and suspended in water for a day to break the boron complex. The final ligand was filtered and dried under vacuum. Yield: 69%. ^{1}H NMR (400 MHz, $CDCl_3$): $\delta=7.65$ (d, $J=15.8$ Hz, 2H), 7.51 (d, $J=3.7$ Hz, 2H), 7.38–7.30 (m, 4H), 6.44 (d, $J=15.7$ Hz, 2H), 5.79 ppm (s, 1H); ^{13}C NMR (75 MHz, [D_6]DMSO): $\delta=183.44$, 138.14, 134.33, 129.67, 127.94, 125.70, 123.86, 101.42 ppm; IR (KBr): $\nu=3419$, 3091, 1623, 1575, 1506, 1417, 1137, 968, 867, 794, 723, 611, 474 cm^{-1}; ESI-MS: $m/z=287$ $[M<\text{M->H}]^-$, 575 $[2M<\text{M->H}]^-$; elemental analysis calcd (%) for 3-thphCCM·1.2H_2O: C 58.3, H 4.37, S 20.8; found: C 58.1, H 4.17, S 20.9.

Physical measurements

C, H, and N analyses were performed with a Pekin-Elmer II Series CHNS/O Analyzer 2400 at the Servei de Microanàlisis del Consell Superior d'Investigació Científiques (CSIC), Barcelona. ^{1}H NMR and ^{13}C NMR spectra were recorded with a Bruker Avance-400 spectrometer. The ESI mass spectra were measured with a spectrometer LC/MSD-TOF (Agilent Technologies) with a double nebulizer source. Infrared spectra (4000–400 cm^{-1}) were recorded from KBr pellets with a Bruker Vector 22 spectrophotometer. Solution UV/Vis absorption spectra were recorded by using a UV/Visible PerkinElmer (Lambda II) spectrophotometer. Solid UV/Vis absorption spectra were recorded by using diffuse reflectance sphere DRA-2500 acces-

sory in a UV/Vis/NIR Varian Cary 5000 spectrophotometer. Only distilled solvents (CH_2Cl_2) were employed and concentrations of compound **1** and **2** were 10×10^{-6} M.

Electrochemistry

Cyclic voltammograms (CV) and differential pulse voltammograms in solution were recorded with a potentiostat SP-150 (BioLogic) modulated with the program EC-Lab V10.02, at the Universitat de Barcelona. A standard three-electrode assembly (glassy carbon working together with auxiliary and reference platinum electrodes) with 0.1×10^{-3} M NBu_4PF_6 as the supporting electrolyte. No IR compensation was employed. Quoted potentials are versus the ferrocene/ferrocenium couple, which was used as an internal standard. The scan rates for cyclic voltammetry (CV) and differential pulse voltammetry (DPV) were 50 and 50–100 mVs^{-1}, respectively. Distilled solvents were employed, and the concentrations of the compounds were approximately 10^{-3} M.

Computational details

Theoretical analysis was performed with the Gaussian code,[34] by using the 03 and 09 versions. It considers optimization of the ground-state geometry of 2-thphCCM (**1**) and 3-thphCCM (**2**) by using the density functional theory (DFT) methodology with the Becke, Lee, Yang, and Parr B3LYP hybrid functional for exchange and correlation effects and the 6–311G+(d,p) basis set. A two-step procedure previously used[25] was implemented to resolve the geometry and energy of the ground state for the several hypothetic conformers of the 2-thphCCM (**1**) and 3-thphCCM (**2**) compounds, both in the gas phase and in solvent, considering the Tomasi polarized continuum model (PCM) to account for the effect of the dichloromethane solvent used in UV/Vis experimental spectra. The vertical $S_0\rightarrow S_n$ ($n=1$ to 5) singlet–singlet transitions corresponding to absorption spectra of each of the 2-thphCCM and 3-thphCCM oligomers were resolved by time-dependent DFT (TD-DFT/B3LYP/6–311G+(d,p)) calculations[26] including the solvent effect. The electronic densities of the HOMO and LUMO states were also obtained. Luminescence spectra were calculated by optimizing the first singlet excited-state structure and studying the vertical transition.

The DFT stretching calculations were performed by using the ADF software package.[35] The dispersion-corrected GGA PBE exchange-correlation functional and the triple-ζ plus polarization (TZP), Slater-type orbital local basis set were used. Dispersion corrections (DFT-D3) were added to the total bonding energy gradient and second derivatives, where applicable, according to the procedure described by Grimme et al.[36] All electrons were taken into account, except for the gold where a large frozen core was used. To account for relativistic effects in the electrodes, the zeroth-order regular approximation (ZORA) to the Dirac equation was used. Geometries were converged to energy changes of less than 10^{-3} hartree, energy gradients of less than 1×10^{-3} hartree/Å maximum and 6.7×10^{-4} hartree/Å RMS. The electrodes were modeled as two gold pyramids terminated with (111) surfaces. Each electrode consisted of five layers, as shown in Figure 7. The initial electrode separation is 2.54 nm, as shown in the left panel. The electrode separation is determined from the distance between the outer gold layers, center-to-center. The calculations were performed as follows. First, the molecular geometry was relaxed for the electrode while keeping the coordinates of the outer three gold layers fixed. Only the inner two layers were allowed to relax. After convergence, the electrodes were pulled outwards, each with a displacement of 0.02 Å, and the geometry was optimized again. This process was repeated until the Au–Au distance reached 4.40 nm.

To correct for well-known correlation errors upon addition/removal of a charge on the molecule, the DFT+Σ method was employed.[37] The Σ correction consists of two parts. First, a correction to the ionization potential and electron affinity is calculated based on gas-phase calculations for the molecule with −1, 0, and +1 electrons. Second, image–charge effects were calculated for the different charge states (also in the gas phase) by using the Hirschfeld atomic charge distribution between two parallel plates. The image planes were set at a distance of 1.5 Å away from the sulfur atoms. Both corrections were implemented as a scissor operator. To compute the transmission, the outer two gold layers were coupled to wide-band limit electrodes.[38]

Electrochemistry measurements on self-assembled monolayers of compound 1 and 2 on gold electrodes

Electrochemical experiments were conducted by using 0.1 M $(NBu_4)(PF_6)$ solutions in dry CH_2Cl_2. Before each measurement, the organic solution was purged with ultrapure N_2 gas for about 10 min. The working electrode was a thin vapor-deposited Au film deposited on glass (12×12 mm slides purchased from Arrandee, Germany). The reference electrode was a platinum wire, and other platinum wire served as the counter electrode. Final redox potentials were referenced to the ferrocene/ferrocenium (Fc/Fc^+) couple. Gold slides (working electrode) were annealed by using a H_2 flame to obtain a preferential Au(111) orientation. After annealing, the Au(111) slides were placed in an ethanol 50×10^{-6} M solution containing 2-thphCCM or 3-thphCCM. The time required to obtain the SAMs was 24 h. After this period, the electrodes were further rinsed with ethanol for 10 min and dried by using a nitrogen flow. The electrodes modified with SAMs were characterized by using cyclic voltammetry (scan rate 50 mVs^{-1}) and differential pulse voltammetry (scan rate 20 $mV\,s^{-1}$, pulse amplitude 25 mV, and a pulse width 50 ms).

Single-molecule conductance measurements

The transport properties of single-molecule junctions were studied by using lithographic mechanically controllable break junctions (MCBJs) in air at room temperature. Details concerning the experimental procedures are given elsewhere.[39] The layout of an MCBJ device in a three-point bending mechanism is shown in Figure 9. The sample is bent by a pushing rod, the vertical movement of which is controlled by a stepper motor in combination with a piezo stack. The moving rate of the electrodes was 0.6 to 6 $nm\,s^{-1}$.

Prior to molecular deposition, we first characterized the gold electrodes at room temperature; we measured the current passing through the MCBJ device at a fixed bias voltage of 0.1 V applied

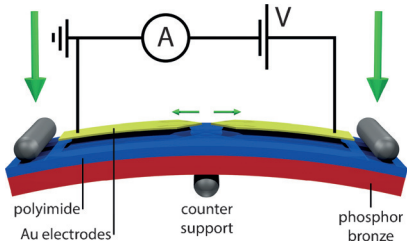

Figure 9. Schematic representation of the MCBJ technique.

across the electrodes, while driving the pushing rod up and down to mechanically break and form the contact. The current was measured with a battery-powered logarithmic amplifier capable of detecting currents over a range of nine orders of magnitude. To obtain statistically significant data, sets of up to 5000 consecutive breaking traces from individual junctions were analyzed numerically without any data selection.

After the initial characterization of the clean junction, deposition of the molecules was performed in situ by pipetting a 1 μL droplet of the target molecule in solution on the gold electrodes. The solution was prepared just before the experiment; the target molecule (0.5×10^{-3} M) was dissolved in dichloromethane. After deposition, we continued to monitor the conductance while breaking and reforming the gold contacts.

Acknowledgments

This work has been funded by the FONDECYT REGULAR grants 1110206, 1140770, and 1140199, PAI-CONICYT 79150041, Conicyt PFCHA 21140734, ANILLO project Act 1117, Millenium Project RC120001, the Dutch funding agencies FOM and NWO/OCW, by the EU through a RISE (DAFNEOX) project, SEP-210165479 by the MICINN of Spain (projects CTQ2012-32247 and MAT2013-47869-C4-2-P). N.A.-A. and R.D.-T. also acknowledge financial support from MINECO through the "Severo Ochoa" Programme for Centres of Excellence in R&D (SEV-2015-0496).

Keywords: curcumin · density functional calculations · differential pulse voltammetry · HOMO–LUMO band gap energies · self-assembly

[1] a) M. Ratner, *Nat. Nanotechnol.* **2013**, *8*, 378 – 381; b) M. Tsutsui, M. Taniguchi, *Sensors* **2012**, *12*, 7259 – 7298.

[2] a) L. Sun, Y. A. Diaz-Fernandez, T. A. Gschneidtner, F. Westerlund, S. Lara-Avila, K. Moth-Poulsen, *Chem. Soc. Rev.* **2014**, *43*, 7378 – 7411; b) S. V. Aradhya, L. Venkataraman, *Nat. Nanotechnol.* **2013**, *8*, 399 – 410; c) Madhuprasad, M. P. Bhat, H. Y. Jung, D. Losic, M. D. Kurkuri, *Chem. Eur. J.* **2016**, *22*, 6148 – 6178.

[3] a) N. J. Tao, *Nat. Nanotechnol.* **2006**, *1*, 173 – 181; b) P. Moreno-García, M. Gulcur, D. Z. Manrique, T. Pope, W. Hong, V. Kaliginedi, C. Huang, A. S. Batsanov, M. R. Bryce, C. Lambert, T. Wandlowski, *J. Am. Chem. Soc.* **2013**, *135*, 12228 – 12240; c) M. Kamenetska, M. Koentopp, A. C. Whalley, Y. S. Park, M. L. Steigerwald, C. Nuckolls, M. S. Hybertsen, L. Venkataraman, *Phys. Rev. Lett.* **2009**, *102*, 126803.

[4] M. L. Perrin, R. Frisenda, M. Koole, J. S. Seldenthuis, J. A. Celis Gil, H. Valkenier, J. C. Hummelen, N. Renaud, F. C. Grozema, J. M. Thijssen, D. Dulić, H. S. J. van der Zant, *Nat. Nanotechnol.* **2014**, *9*, 830 – 834.

[5] a) L. Venkataraman, J. E. Klare, C. Nuckolls, M. S. Hybertsen, M. L. Steigerwald, *Nature* **2006**, *442*, 904 – 907; b) B. Capozzi, E. J. Dell, T. C. Berkelbach, D. R. Reichman, L. Venkataraman, L. M. Campos, *J. Am. Chem. Soc.* **2014**, *136*, 10486 – 10492; c) A. C. Aragonès, N. Darwish, J. Im, B. Lim, J. Choi, S. Koo, I. Díez-Pérez, *Chem. Eur. J.* **2015**, *21*, 7716 – 7720.

[6] E. Leary, A. La Rosa, M. T. Gonzalez, G. Rubio-Bollinger, N. Agraït, N. Martin, *Chem. Soc. Rev.* **2015**, *44*, 920 – 942.

[7] A. Coskun, J. M. Spruell, G. Barin, W. R. Dichtel, A. H. Flood, Y. Y. Botros, J. F. Stoddart, *Chem. Soc. Rev.* **2012**, *41*, 4827 – 4859.

[8] a) F. Chen, X. Li, J. Hihath, Z. Huang, N. Tao, *J. Am. Chem. Soc.* **2006**, *128*, 15874 – 15881; b) M. Tsutsui, M. Taniguchi, T. Kawai, *J. Am. Chem. Soc.* **2009**, *131*, 10552 – 10556; c) J. Ponce, C. R. Arroyo, S. Tatay, R. Frisenda, P. Gaviña, D. Aravena, E. Ruiz, H. S. J. van der Zant, E. Coronado, *J. Am. Chem. Soc.* **2014**, *136*, 8314 – 8322; d) V. Kaliginedi, A. V. Rudnev, P. Moreno-García, M. Baghernejad, C. Huang, W. Hong, T. Wandlowski, *Phys. Chem. Chem. Phys.* **2014**, *16*, 23529 – 23539; e) Z. Li, M. Smeu, M. A. Ratner, E. Borguet, *J. Phys. Chem. C* **2013**, *117*, 14890 – 14898; f) Y. S. Park, A. C. Whalley, M. Kamenetska, M. L. Steigerwald, M. S. Hybertsen, C. Nuckolls, L. Venkataraman, *J. Am. Chem. Soc.* **2007**, *129*, 15768 – 15769; g) Y. Zhao, S. Lindsay, S. Jeon, H.-J. Kim, L. Su, B. Lim, S. Koo, *Chem. Eur. J.* **2013**, *19*, 10832 – 10835; h) I. Rattalino, V. Cauda, P. Motto, T. Limongi, G. Das, L. Razzari, F. Parenti, E. Di Fabrizio, A. Mucci, L. Schenetti, G. Piccininib, D. Demarchiab, *RSC Adv.* **2012**, *2*, 10985 – 10993; i) Y. S. Park, J. R. Widawsky, M. Kamenetska, M. L. Steigerwald, M. S. Hybertsen, C. Nuckolls, L. Venkataraman, *J. Am. Chem. Soc.* **2009**, *131*, 10820 – 10821; j) M. Gulcur, P. Moreno-García, X. Zhao, M. Baghernejad, A. S. Batsanov, W. Hong, M. R. Bryce, T. Wandlowski, *Chem. Eur. J.* **2014**, *20*, 4653 – 4660.

[9] a) Y. Ie, K. Tanaka, A. Tashiro, S. K. Lee, H. R. Testai, R. Yamada, H. Tada, Y. Aso, *J. Phys. Chem. Lett.* **2015**, *6*, 3754 – 3759; b) Y. Ie, T. Hirose, H. Nakamura, M. Kiguchi, N. Takagi, M. Kawai, Y. Aso, *J. Am. Chem. Soc.* **2011**, *133*, 3014 – 3022.

[10] a) N. Aliaga-Alcalde, L. Rodriguez, M. Ferbinteanu, P. Hofer, T. Weyhermuller, *Inorg. Chem.* **2012**, *51*, 864 – 873; b) N. Aliaga-Alcalde, P. Marques-Gallego, M. Kraaijkamp, C. Herranz-Lancho, H. den Dulk, H. Gorner, O. Roubeau, S. J. Teat, T. Weyhermuller, J. Reedijk, *Inorg. Chem.* **2010**, *49*, 9655 – 9663; c) F. Kuhlwein, K. Polborn, W. Z. Beck, *Z. Anorg. Allg. Chem.* **1997**, *623*, 1211 – 1219; d) K. Krishnankutty, V. D. John, *Synth. React. Inorg. Met.-Org. Chem.* **2003**, *33*, 343 – 358; e) M. Menelaou, T. Weyhermuller, M. Soler, N. Aliaga-Alcalde, *Polyhedron* **2013**, *32*, 398 – 405; f) B. Banik, K. Somyajit, G. Nagaraju, A. R. Chakravarty, *Dalton Trans.* **2014**, *43*, 13358 – 13369; g) X. Lei, W. Su, P. Li, Q. Xiao, S. Huang, Q. Qian, C. Huang, D. Qin, H. Lan, *Polyhedron* **2014**, *81*, 614 – 618; h) B. Balaji, B. Balakrishnan, S. Perumalla, A. A. Karande, A. R. Chakravarty, *Eur. J. Med. Chem.* **2014**, *85*, 458 – 467.

[11] a) M. Menelaou, F. Ouharrou, L. Rodriguez, O. Roubeau, S. J. Teat, N. Aliaga-Alcalde, *Chem. Eur. J.* **2012**, *18*, 11545 – 11549; b) Y. Mawani, C. J. Orvig, *J. Inorg. Biochem.* **2014**, *132*, 52 – 58.

[12] a) C. C. Chignell, P. Bilski, K. J. Reszka, A. G. Motten, R. H. Sik, T. A. Dahl, *Photochem. Photobiol.* **1994**, *59*, 295 – 302; b) S. M. Khopde, K. I. Priyadarsini, D. K. Palit, R. Mukherjee, *Photochem. Photobiol.* **2000**, *72*, 625 – 631; c) L. Nardo, R. Paderno, A. Andreoni, M. Másson, T. Haukvik, H. H. Tønnesen, *Spectroscopy* **2008**, *22*, 187 – 198; d) K. I. Priyadarsini, *J. Photochem. Photobiol. C* **2009**, *10*, 81 – 95; e) L. Nardo, A. Andreoni, M. Bondani, M. Másson, T. Haukvik, H. H. Tønnesen, *J. Fluoresc.* **2012**, *22*, 597 – 608; f) F. Payton, P. Sandusky, W. L. Alworth, *J. Nat. Prod.* **2007**, *70*, 143 – 146.

[13] a) H. H. Tønnesen, J. Karlsen, A. Mostad, *Acta Chem. Scand. B* **1982**, *36*, 475 – 479; b) J. T. Mague, W. L. Alworth, F. L. Payton, *Acta Crystallogr. Sect. A* **2004**, *60*, o608 – o610; c) S. P. Parimita, Y. V. Ramshankar, S. Suresh, T. N. Guru Row, *Acta Crystallogr. Sect. A* **2007**, *63*, o860-o862.

[14] J. Zhou, Y. X. Yang, P. Liu, N. Camillone, M. G. White, *J. Phys. Chem. C* **2010**, *114*, 13670 – 13677.

[15] F. Prins, A. Barreiro, J. W. Ruitenberg, J. S. Seldentuis, N. Aliaga-Alcalde, L. M. K. Vandersypen, H. S. J. van der Zant, *Nano Lett.* **2011**, *11*, 4607 – 4611.

[16] In the calculation of the HOMO–LUMO energies, the ionization potential energies correspond to the HOMO energy together with the electron–electron repulsion of the same orbital. An identical approach was taken for the calculation of the optical energies.

[17] C. B. George, M. A. Ratner, J. B. Lambert, *J. Phys. Chem. A* **2009**, *113*, 3876 – 3880.

[18] a) H. J. J. Pabon, *Recl. Trav. Chim. Pays-Bas* **1964**, *83*, 379 – 386; b) U. Pedersen, P. B. Rasmussen, S.-O. Lawesson, *Liebigs Ann. Chem.* **1985**, *1985*, 1557 – 1569.

[19] a) D. Liu, C. Gu, M. Xiao, M. Qiu, M. Sun, R. Yang, *Polym. Chem.* **2015**, *6*, 3398 – 3406; b) Q. Fan, Y. Liu, M. Xiao, H. Tan, Y. Wang, W. Su, D. Yu, R. Yang, W. Zhu, *Org. Electron.* **2014**, *15*, 3375 – 3383; c) N. Atilgan, F. Algi, A. M. Önall, A. Cihaner, *Tetrahedron* **2009**, *65*, 5776 – 5781; d) C. Y. Yu, C. P. Chen, S. H. Chan, G. W. Hwang, C. Ting, *Chem. Mater.* **2009**, *21*, 3262 – 3269.

[20] a) A. P. Kulkami, C. J. Tonzola, A. Babel, S. A. Jenekhe, *Chem. Mater.* **2004**, *16*, 4556 – 4573; b) J. Pommerehne, H. Westweber, W. Guss, R. F. Mahrt, H. Bässler, M. Porsch, J. Daub, *Adv. Mater.* **1995**, *7*, 551 – 554; c) P. I. Djurovich, E. I. Mayo, S. R. Forrest, M. E. Thompson, *Org. Electron.* **2009**, *10*, 515 – 520; d) The onset potentials are determined from the intersection

of the tangents between the base line and the signal current; e) N. Connelly, W. E. Geiger, *Chem. Rev.* **1996**, *96*, 877 – 910.

[21] a) F. Zsila, Z. Bikádi, M. Simonyi, *Biochem. Biophys. Res. Commun.* **2003**, *301*, 776 – 782.

[22] a) R. Adhikary, P. Mukherjee, T. W. Kee, J. W. Petrich, *J. Phys. Chem. B* **2009**, *113*, 5255 – 5261; b) R. K. Saini, K. Das, *J. Lumin.* **2014**, *145*, 832 – 837.

[23] a) T. Koopmans, *Physica* **1934**, *1*, 104 – 113; b) O. Gritsenko, E. J. Baerends, *Can. J. Chem.* **2009**, *87*, 1383 – 1391; c) D. P. Chong, O. V. Gritsenko, E. J. Baerends, *J. Chem. Phys.* **2002**, *116*, 1760; d) O. V. Gritsenko, E. J. Baerends, *J. Chem. Phys.* **2002**, *117*, 9154 – 9159.

[24] a) A. D. Becke, *J. Chem. Phys.* **1993**, *98*, 5648 – 5652; b) C. Lee, W. Yang, R. G. Parr, *Phys. Rev. B* **1988**, *37*, 785 – 789.

[25] F. Martínez, G. Neculqueo, S. O. Vásquez, R. Letelier, M. T. Garland, A. Ibañez, J. C. Bernede, *J. Mol. Struct.* **2010**, *973*, 56 – 61.

[26] G. Neculqueo, V. Rojas-Fuentes, A. Lopez, R. Matute, S. O. Vásquez, F. Martínez, *Struct. Chem.* **2012**, *23*, 1751 – 1760.

[27] a) A. D. McLean, G. S. Chandler, *J. Chem. Phys.* **1980**, *72*, 5639 – 5648; b) J.-P. Blaudeau, M. P. McGrath, L. A. Curtiss, L. Radom, *J. Chem. Phys.* **1997**, *107*, 5016 – 5021; c) A. J. H. Wachters, *J. Chem. Phys.* **1970**, *52*, 1033 – 1036; d) P. J. Hay, *J. Chem. Phys.* **1977**, *66*, 4377 – 4384; e) K. Raghavachari, G. W. Trucks, *J. Chem. Phys.* **1989**, *91*, 1062 – 1065; f) R. C. Binning, Jr., L. A. Curtiss, *J. Comput. Chem.* **1990**, *11*, 1206 – 1216; g) M. P. McGrath, L. Radom, *J. Chem. Phys.* **1991**, *94*, 511 – 516; h) L. A. Curtiss, M. P. McGrath, J.-P. Blaudeau, N. E. Davis, R. C. Binning, Jr., L. Radom, *J. Chem. Phys.* **1995**, *103*, 6104 – 6113.

[28] T. Clark, J. Chandrasekhar, G. W. Spitznagel, P. v. R. Schleyer, *J. Comput. Chem.* **1983**, *4*, 294 – 301.

[29] M. J. Frisch, J. A. Pople, J. S. Binkley, *J. Chem. Phys.* **1984**, *80*, 3265 – 3269.

[30] a) I. Ponce, J. F. Silva, R. Oñate, M. Caroli, M. A. Paez, J. H. Zagal, J. Pavez, *J. Phys. Chem. C* **2012**, *116*, 15329 – 15341; b) J. Noh, E. Ito, T. Araki, M. Hara, *Surf. Sci.* **2003**, *532*, 1116 – 1120.

[31] T. Ikeda, Y. Nagata, Y. Zheng, D. Liu, H. J. Butt, M. Shimoda, *Langmuir* **2014**, *30*, 1536 – 1542.

[32] C. A. Martin, D. Ding, H. S. J. van der Zant, J. M. van Ruitenbeek, *New J. Phys.* **2008**, *11*, 065008 – 065026.

[33] M. Büttiker, Y. Imry, R. Landauer, S. Pinhas, *Phys. Rev. B* **1985**, *31*, 6207 – 6215.

[34] Gaussian 09, Revision A.01, M. J. Frisch, G. W. Trucks, H. B. Schlegel, G. E. Scuseria, M. A. Robb, J. R. Cheeseman, G. Scalmani, V. Barone, B. Mennucci, G. A. Petersson, H. Nakatsuji, M. Caricato, X. Li, H. P. Hratchian,A. F. Izmaylov, J. Bloino, G. Zheng, J. L. Sonnenberg, M. Hada, M. Ehara, K. Toyota, R. Fukuda, J. Hasegawa, M. Ishida, T. Nakajima,Y. Honda, O. Kitao, H. Nakai, T. Vreven, J. A. Montgomery, Jr.,J. E. Peralta, F. Ogliaro, M. Bearpark, J. J. Heyd, E. Brothers,K. N. Kudin, V. N. Staroverov, R. Kobayashi, J. Normand, K. Raghavachari, A. Rendell, J. C. Burant, S. S. Iyengar, J. Tomasi, M. Cossi, N. Rega, J. M. Millam, M. Klene, J. E. Knox, J. B. Cross,V. Bakken, C. Adamo, J. Jaramillo, R. Gomperts, R. E. Stratmann,O. Yazyev, A. J. Austin, R. Cammi, C. Pomelli, J. W. Ochterski, R. L. Martin, K. Morokuma, V. G. Zakrzewski, G. A. Voth,P. Salvador, J. J. Dannenberg, S. Dapprich, A. D. Daniels, O. Farkas, J. B. Foresman, J. V. Ortiz, J. Cioslowski, D. J. Fox, Gaussian, Inc., Wallingford, CT, **2009**.

[35] a) G. te Velde, F. M. Bickelhaupt, S. J. A. van Gisbergen, C. Fonseca Guerra, E. J. Baerends, J. G. Snijders, T. Ziegler, *J. Comput. Chem.* **2001**, *22*, 931 – 967; b) C. Fonseca Guerra, J. G. Snijders, G. te Velde, E. J. Baerends, *Theor. Chem. Acc.* **1998**, *99*, 391 – 403.

[36] S. Grimme, S. Ehrlich, L. Goerigk, *J. Comput. Chem.* **2011**, *32*, 1456 – 1465.

[37] S. Y. Quek, L. Venkataraman, H. J. Choi, S. G. Louie, M. S. Hybertsen, J. B. Neaton, *Nano Lett.* **2007**, *7*, 3477 – 3482.

[38] C. J. O. Verzijl, J. S. Seldenthuis, J. M. Thijssen, *J. Chem. Phys.* **2013**, *138*, 094102.

[39] C. A. Martin, D. Ding, H. S. J. van der Zant, J. M. van Ruitenbeek, *New J. Phys.* **2008**, *11*, 065008.

Received: March 12, 2016
Published online on July 26, 2016